Brazilian Journal of Chemical Engineering (2021) 38:351–359
https://doi.org/10.1007/s43153-021-00097-3

ORIGINAL PAPER

Siderite decomposition at room temperature conditions for CO_2 capture applications

Eduin Yesid Mora Mendoza[1,2] · Armando Sarmiento Santos[1] · Enrique Vera López[1] · Vadym Drozd[2] · Andriy Durygin[2] · Jiuhua Chen[2] · Surendra K. Saxena[2]

Received: 21 October 2020 / Revised: 27 January 2021 / Accepted: 5 April 2021 / Published online: 19 April 2021

Abstract

The decomposition of synthetic siderite ($FeCO_3$) in air atmosphere at room temperature conditions was studied. Siderite was formed by mechanochemical reaction of Fe_3O_4 and graphite at high CO_2 pressure in the presence of water. Kinetics of decomposition reaction was studied over period up to 9 days and it is shown that decomposition reaction obeys geometrical contraction solid-state reaction mechanism model. It was found that the water influences not only the kinetics of siderite formation but also its stability. Siderite completely decomposes at ambient conditions yielding magnetite (Fe_3O_4) and hematite (Fe_2O_3) which can reversibly re-absorb carbon dioxide.

Keywords Mechanochemical reaction · Room temperature decomposition · Kinetics of siderite decomposition · Efficient reversible absorbent of CO_2

Introduction

During the last two centuries and mainly the last several decades Earth has warmed as a result of increasing emissions of green-house effect gases to the atmosphere (Pannoccia et al. 2007; Cheng-Hsiu et al. 2012). These gases include carbon dioxide (CO_2), methane (CH_4), nitrous oxide (N_2O), hydrofluorocarbons (HFC), perfluorocarbons (PFCs) and sulphur hexafluoride (SF_6). Among of these, carbon dioxide is considered the main cause of global warming. Two major contributors to CO_2 emission are different sectors of industry which utilize fossil fuel and forest fires (Cheng-Hsiu et al. 2012; Han et al. 2014; Kumar et al. 2015a; Merkel et al. 2009). It is predicted that by the year 2100 the CO_2 concentration in atmosphere could reach 570 ppm, causing further increase of global temperature, sea level rise and extinction of many living species (Yan et al. 2008; Stewart and Hessami 2005).

✉ Eduin Yesid Mora Mendoza
eduin.mora@uptc.edu.co

[1] Universidad Pedagógica y Tecnológica de Colombia UPTC, 150008 Tunja, Colombia

[2] Center for the Study of Matter at Extreme Conditions, College of Engineering and Computing, Florida International University, Miami, FL 33199, USA

Although most countries are aware of this situation, today there are no large-scale developments to predict that this problem is close to being solved. This, due to the high costs and in most cases, the technologies used has not been integrated to the expected level (Mora et al. 2019a). Organizations as National Energy Technology Laboratory (NETL), are pursuing efforts of the governments, industrial sector and research community, which are focused on developing technologies to reduce emissions of CO_2, its separation and capture, and long-term storage (Figueroa et al. 2008). Carbon dioxide capture and sequestration are promising technologies to reduce atmospheric concentration of CO_2.

Selection of technology for CO_2 capture in industrial sector depends on the type of plant and flue gas composition. For example in power generation, the possible configurations are pre-combustion capture, post-combustion capture, oxy-fuel combustion capture and chemical combustion capture, and each the gas stream to be treated has its specific conditions of pressure, temperature and CO_2 concentration (Zaman and Lee 2013).

The most studied methods to deal with CO_2 are chemical and physical absorption, adsorption, membrane separations, and several novel separation techniques (Pannoccia et al. 2007; Zaman and Lee 2013). Chemical absorption is the most mature technology, although it has important disadvantages as low CO_2 absorption capacity, thermal degradation

and corrosive nature of the absorbents (Han et al. 2014). Amines, ammonia and potassium carbonate are mainly used in chemical absorption technology (Zaman and Lee 2013; Bello and Idem 2005; Cullinage and Rochelle 2004). Microgel particles have been studied for enhancing of efficiency of amines (Yang et al. 2020). Physical absorption method uses solvents as Selexol, Rectisol, Fluor, Purisol and Sulfolane (Breckenridge et al. 2000) and operates more efficiently at low temperatures and high pressures (Zaman and Lee 2013). Although adsorption has not been commercialized yet, it has attracted a lot of attention because of low energy requirements for adsorbent regeneration and wide temperature range for operation (from room temperature up to 700 °C) (Zaman and Lee 2013). Adsorption can have physical or chemical nature. The regeneration of adsorbents is based on techniques using pressure, vacuum, hybrid vacuum–pressure and electricity methods (Zhang and Webley 2008). Membranes act as filters to separate CO_2 from other gas components. Although it has been shown that the membranes could offer advantages by reducing energy requirements and cost compared with amine technology, this technology is still at laboratory-scale level due to operational problems, contamination, and implementation on large sc (Stewart and Hessami 2005) ale at power plants applications (Folger 2013). Latest research works have revealed important improvements in membranes performance for CO_2 capture from coalbed methane (Zhang et al. 2010) or using polymeric thin films (Xie et al. 2019; Han and Winston Ho 2018). Cryogenics and micro algal are identified as other novel separation techniques, which are being studied in preliminary phases (Song et al. 2019).

Potential use for CO_2 capture of compounds as Mg_2SiO_4, Mg_2VO_4, and Mg_2GeO_4 is under study (Kang 2020). Recently, carbonation of some metal oxides such as MgO, FeO, ZnO has been studied due to favourable thermodynamics of CO_2 absorption reaction and their abundance in nature (Kumar and Saxena 2014). After carbonation the material (metal carbonate) is heated in order to released CO_2 and regenerate the oxide, which can be used in another cycle of carbonation/calcination (Salvador et al. 2003).

Siderite has gained a remarkable interest among researchers because it is a suitable source of iron for industrial processes (Feng et al. 2011; Patterson 1994). Normally, natural siderite contains different amounts of Mg, Ca, Mn impurities (Gotor et al. 2000). Solid solutions with carbonates of Mg and Mn exist in all range of concentrations, while a wide miscibility gap reported between carbonates of Fe and Ca (Mora et al. 2019a). Synthetic siderite can be obtained either by wet chemistry methods or at high temperature high pressure conditions by reactions of iron oxides, particularly Fe_3O_4 or Fe_2O_3, and carbon dioxide (Chai 1994; Das 2016; Zhou 2011). These iron oxides have important use in blast furnace for steel fabrication.

There are several studies about mechanism of thermal decomposition of siderite which report Fe_3O_4, FeO, α-Fe_2O_3 and γ-Fe_2O_3 as major products of decomposition (Feng et al. 2011; Alkaç and Atalay 2008; Fosbøl et al. 2010; Kumar et al. 2015b). Formation of specific product depends on the atmosphere, chemical composition of the siderite sample (presence impurities), and synthesis history (Feng et al. 2011; Gotor et al. 2000; Alkaç and Atalay 2008; Fosbøl et al. 2010). Under flow of oxygen, oxidation occurs rapidly and Fe_2O_3 is formed while in inert atmosphere or vacuum Fe_3O_4 and FeO or Fe_2O_3 are detected at moderate (Feng et al. 2011; Gotor et al. 2000; Alkaç and Atalay 2008) and high temperatures (Gallagher and Warne 1981), respectively. Moreover, the temperatures of thermal decomposition of synthetic and natural samples of siderite are different. Decomposition temperature of synthetic siderite is approximately 200 K lower than that one of the natural sample (Gotor et al. 2000).

This paper presents results on CO_2 capture using Fe_3O_4 as an absorbent. Siderite is a product of mechanochemical reaction between gaseous CO_2 and solid Fe_3O_4. Effect of water on the chemical stability of siderite (carbon dioxide desorption properties) is studied. Reactions (1) and (2) correspond to the carbonation and decomposition reactions respectively, which were studied in this work.

$$2Fe_3O_4(s) + C(s) + 5CO_2(g) \rightarrow 6FeCO_3(s) \quad (1)$$

$$3FeCO_3(s) + 1/2O_2 \rightarrow Fe_3O_4(s) + 3CO_2(g) \quad (2)$$

Experimental

Planetary ball mill Retsch PM100 operating at 400 revolutions per minute was used to establish mechanochemical reaction between magnetite and carbon dioxide at room temperature and elevated CO_2 pressure (10–30 bar). Reaction vessel was a stainless-steel jar of 50 mL volume capable for holding up to 100 bar gas pressure. High purity CO_2 gas (Airgas, 99.999%) was loaded into the reactor at different pressures together with 3.00 g of magnetite (Alfa Aesar, nanopowder, 97%) and graphite (Alfa Aesar CD Graphite powder, crystalline, 325 mesh, 99%) mixture (molar ratio 2:1, according reaction (1)). Water (3.0 ml) was added to the mixture of magnetite and graphite. The powder to balls (stainless steel) weight ratio was 2:27. Reactor was flushed several times with CO_2 gas to ensure a pure CO_2 atmosphere inside the reactor. Mechanochemical reaction was run for 36 h. Each 1 h milling interval was followed by half an hour cooling interval to avoid overheating of the sample, which can affect the stability of siderite.

Thermogravimetric analysis (TGA) and differential scanning calorimetry (DSC) were conducted in a temperature

range of 25–1000 °C using TA Instruments SDT Q600 instrument. Experiments were performed in air and Ar atmospheres with a heating rate of 10 °C/min.

Powder X-ray diffraction patterns were collected using Bruker GADDS/D8 diffractometer equipped with Apex Smart CCD Detector and molybdenum rotating anode. Collected 2D diffraction patterns were integrated using Fit2D software (Hammersley 1997). Quantitative phase analysis of the samples was performed using Rietveld method and GSAS package (Toby 2001; Larson and Dreele 2004). The CO_2 sorption capacity was calculated using the results generated by Rietveld refinement of XRD patterns. Surface area of the powders was measured using Brunauer–Emmett–Teller (BET) method and Micrometrics Tristar II 3020 instrument.

Results

Thermodynamic simulations in the system Fe_3O_4-C-CO_2

FACTSAGE software and the databases therein, FACT—F*A*C*T 5.0, SGPS—SGTE and SGSL (Bale et al. 2002) were used for thermodynamic modelling in Fe_3O_4-C-CO_2 system. Figure 1 shows the calculated equilibrium temperature as a function of CO_2 pressure in the system Fe_3O_4-C-CO_2-H_2O with different amounts of water, according reaction (1). The results indicate that the siderite formation is favored either by high CO_2 pressures at a constant temperature or by low temperatures at a constant CO_2 pressure (Mora et al. 2019a). Moreover, results reveal that siderite stability depends strongly on water amount in the mixture. As can be seen, equilibrium temperature decreases with the increasing amount of water, which suggests that the regeneration of material is possible at relatively low temperatures.

Siderite formation

Kinetics of iron (II) carbonate formation in mechanochemical reactions between magnetite or hematite and metallic iron as reducing agent was studied in (Mora et al. 2019a). Carbonation of iron ore in mechanochemical reactions was studied (Mora et al. 2019b). It was shown that magnetite carbonation under mechanochemical activation can not be accomplished in the absence of water using graphite as reducing agent due to kinetics limitations. It was demonstrated that water acts as a catalyst in carbonation reactions promoting the formation of CO_3^{2-} and H^+ ions (Kumar et al. 2015a, b).

The XRD pattern of the reaction products after 36 h ball milling at 400 rpm and 30 bar CO_2 pressure is shown in Fig. 2. XRD pattern reveals the presence of siderite (JCPDS # 00-029-0696) as the major phase and minor amount of unreacted magnetite. Amount of the siderite, which was obtained by the Rietveld refinemenet of XRD pattern, is 85.86% that is equivalent to 0.4829 g CO_2/g sorbent absorption capacity and 78.82% of magnetite-to-siderite conversion.

Calculated lattice parameters of siderite are $a=b=4.6638$ (3) Å and $c=15.6744$ (7) Å, which are in good agreement published data (Mora et al. 2019a). Average crystallite size of $FeCO_3$ after 36 h ball milling was estimated using Scherrer's formula and is equal to108 Å.

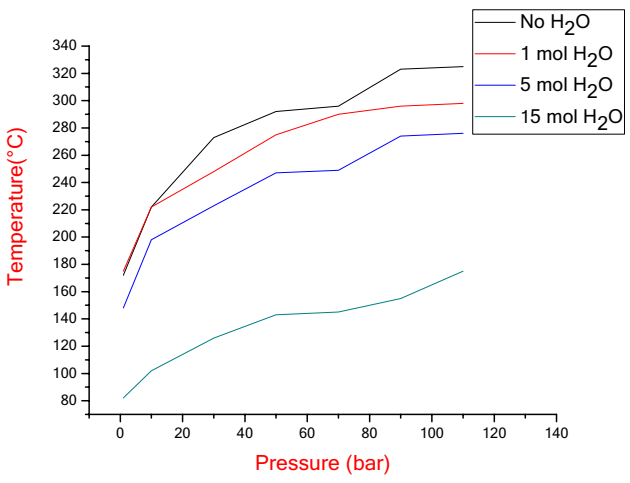

Fig. 1 Equilibrium temperature of siderite decomposition as a function of CO_2 pressure for the system Fe_3O_4-C-CO_2-H_2O with different amounts of water

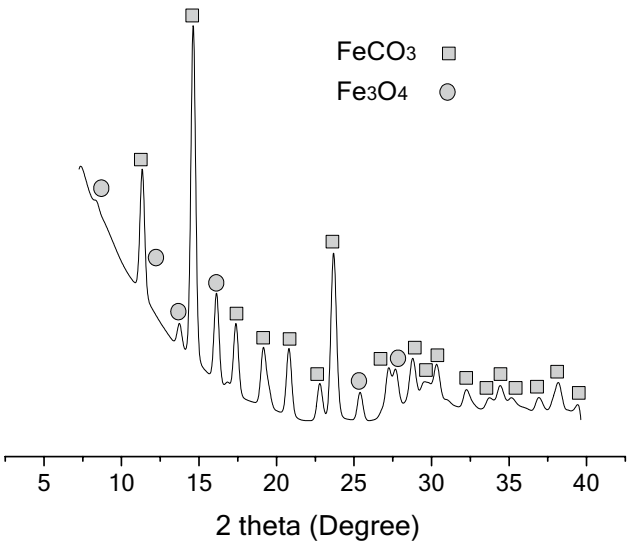

Fig. 2 XRD pattern of Fe_3O_4+C mixture after 36 h of ball milling (400 rpm) at 30 bar CO_2 pressure

Siderite decomposition

Siderite decomposition reactions were studied at room and high temperature (by TG/DCS) conditions. Figure 3 shows the TG/DCS plots of the siderite in argon and air atmospheres.

Weight loss below 100 °C for both samples can be related mainly to the loss of water. As it is evident from DTG curves, highest rate of siderite decomposition is achieved at 263 °C and 343 °C in Ar and air atmospheres, respectively. Higher decomposition temperatures of siderite in air compared to inert atmosphere have been reported previously by others, e.g. (Mora et al. 2019a, b; Alkaç and Atalay 2008). Moreover, these decomposition temperatures of the siderite obtained in the presence of water are lower than decomposition temperature of the siderite synthesized from magnetite and metallic iron by mechanochemical reaction at dry condition [367 °C and 407 °C in Ar and air atmospheres, respectively (Mora et al. 2019a)].

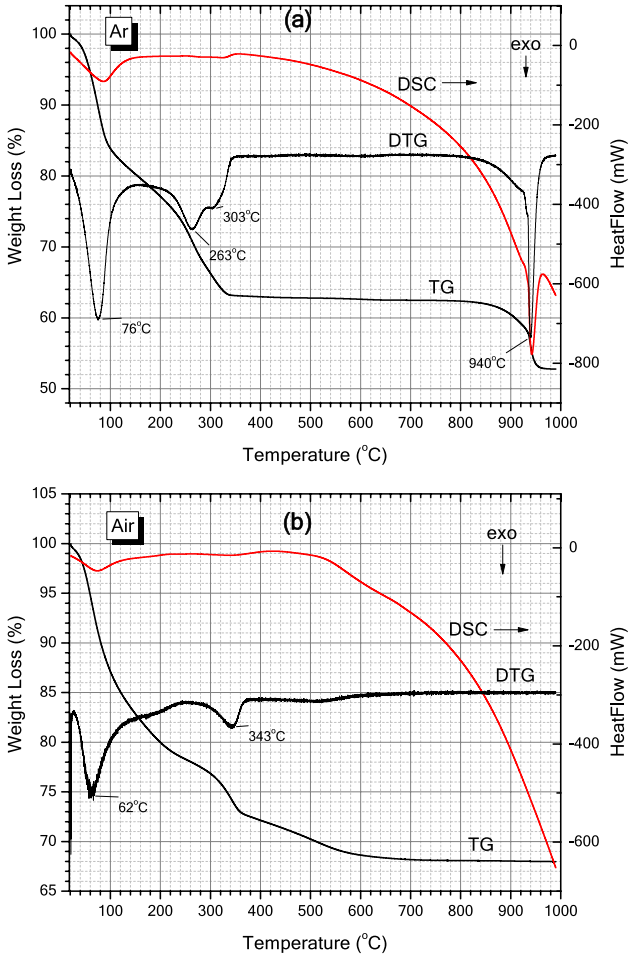

Fig. 3 TG-DSC curves of siderite (formed in Fe_3O_4+C reaction at 30 bar CO_2 pressure, 400 rpm, 36 h) in Ar (**a**) and air (**b**) atmospheres at 10 °C/min heating rate

Formation of non-stoichiometric wustite, FeO, is the first step of siderite decomposition (Mora et al. 2019a), as follows:

$$FeCO_3(s) \rightarrow FeO\,(s) + CO_2(g) \quad (3)$$

Depending on experimental conditions, other products can form from FeO because of its instability below 563 °C (Ding et al. 1998). In inert atmosphere FeO disproportionate producing Fe_3O_4 and Fe:

$$4FeO\,(s) \rightarrow Fe_3O_4(s) + Fe\,(s) \quad (4)$$

In oxygen atmosphere, siderite is oxidized rapidly, yielding Fe_3O_4 according reaction (2) and hematite as follows:

$$4FeCO_3(s) + O_2(g) \rightarrow 2Fe_2O_3(s) + 4CO_2(g) \quad (5)$$

At low oxygen partial pressure, $FeCO_3$ can decompose in the presence of the graphite buffer as follows:

$$3FeCO_3(s) \rightarrow Fe_3O_4(s) + 3C\,(s) + 5/2O_2(g) \quad (6)$$

Thermogravimetry plot in Fig. 3a, reveals that the release of CO_2 by siderite in Ar atmosphere, starts at relatively low temperature (close to 100 °C), presenting the maximum rate at 263 °C. According to TG plot, the total weight loss in the first step of siderite decomposition is 20.3% calculated at corresponding temperature of 303 °C. As can be calculated from Fig. 3b, the experimental total weight loss in air atmosphere is 13.2%, taking account 343 °C as the final siderite decomposition temperature. This loss weight is less than the one in inert atmosphere, due to decomposition of $FeCO_3$ in air is accompanied by iron oxidation to Fe_2O_3 and Fe_3O_4 according to reactions (2) and (5). (Weight loss in reactions (3) and (5) are 37.99% and 31.08% respectively).

In air atmosphere weight loss at higher temperatures with a maximum rate of loss at 550 °C can be related to the oxidation of unreacted carbon which was added to magnetite as a reducing agent. The same carbon acts as a reducing agent in inert atmosphere reducing iron oxides (Fe_2O_3 and Fe_3O_4) to FeO or even to elemental iron. These reduction reactions are accompanied by the weight loss above 900 °C in Ar atmosphere.

Prior to CO_2 release at high temperature, the hydrated material losses absorbed and bound water. Ball milling transfers kinetic energy to material leading to the generation of crystal defects such as vacancies, dislocations and grain boundaries (Ding et al. 1998; Kumar 2014). Moreover, the ball milling decreases the diffusion distance (Gheisari et al. 2009) and creates active sites on the surface of material increasing the surface area (Mora et al. 2019a, b). These effects facilitate decomposition reaction by lowering the diffusion distance and enhancing the diffusivity (Gheisari et al. 2009) in material.

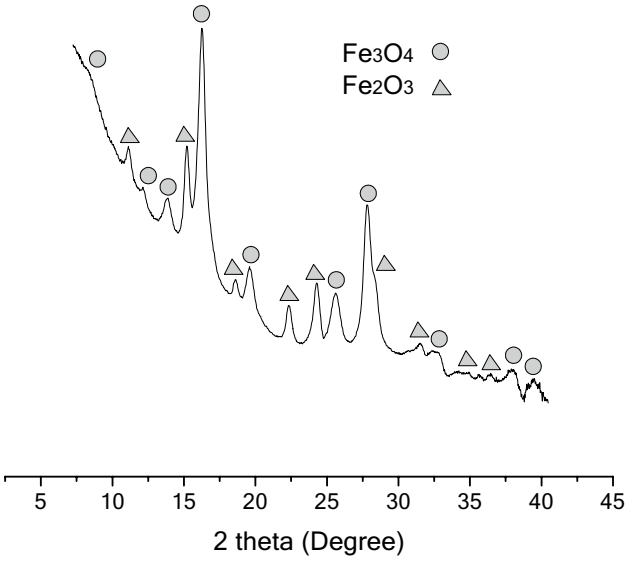

Fig. 4 XRD pattern of decomposed siderite at 400 °C in air for 1 h

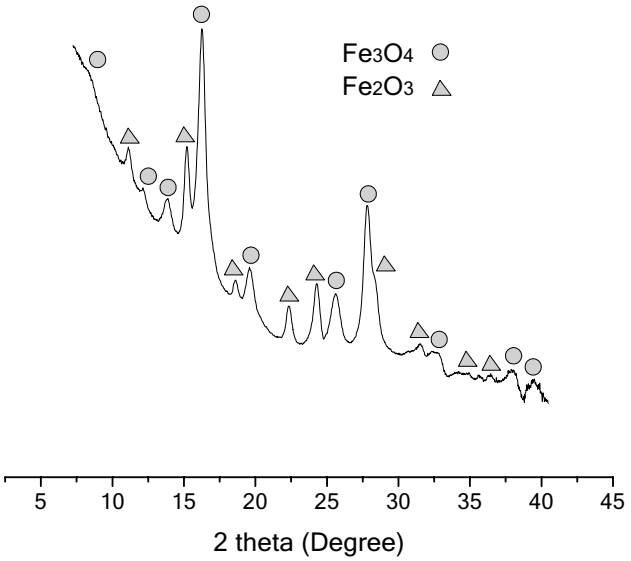

Fig. 5 XRD pattern of spontaneously decomposed siderite after 24 h exposure to air at room temperature

Figure 4 shows the X-ray diffraction pattern of the products of siderite decomposition in air at 400 °C. Magnetite and hematite are detected as decomposition product of siderite proving the discussed above decomposition reactions (2) and (5).

Siderite decomposition was also studied at room temperature conditions (20 °C) in air atmosphere. Material after carbonation reactions was grinded using mortar and pestle and left at room temperature in air for different periods of time. After 24 h exposure time amount of siderite in the sample decreased to 68.48% (see Fig. 5 for XRD pattern of decomposition product), that is 17.38% reduction compared with initial siderite content after carbonation reaction. Magnetite concentration in the sample increased evidencing the decomposition of siderite at room temperature conditions according to reaction (2).

Table 1 $FeCO_3$ weight fraction after different reaction time

Reaction time (h)	$FeCO_3$ weight fraction (%)
24	68.48
48	52.59
72	37.13
96	29.35
120	21.96
144	15.64
168	9.98
192	4.88
216	0.77

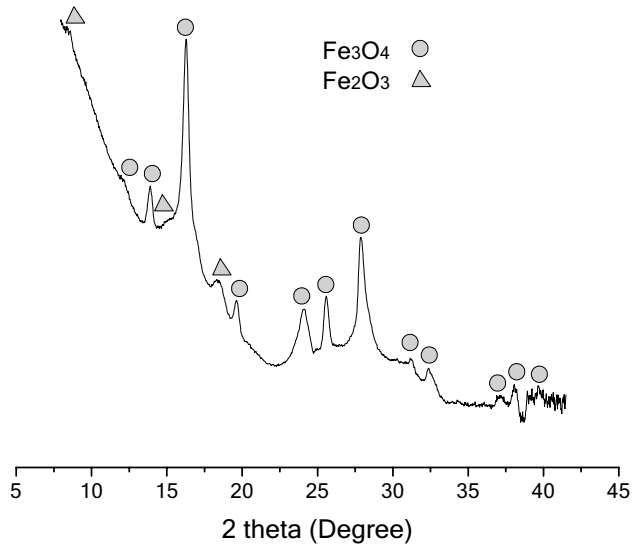

Fig. 6 XRD pattern of spontaneously decomposed siderite (216 h decomposition time)

Changes in the composition of the siderite sample were studied for longer reaction times up to 216 h (9 days) by recording X-ray diffraction patterns every 24 h. Table 1 summarizes results of this study by showing weight fraction of undecomposed siderite in the sample.

As can be seen, after 216 h of spontaneous decomposition siderite in the sample has practically vanished. Figure 6 shows XRD pattern of the sample after 216 h exposure to ambient atmosphere. This pattern reveals presence of hematite (JCPDS # 00-089-2810) that can be associated to magnetite oxidation according to reaction (7). Lack of reducing agent and intermediate products after capture CO_2 process reveals the suitable efficiency of carbonation reactions. Next

Table 2 CO_2 capture capacity of sorbent, reaction time to decompose the siderite and the extra substances added, in second, third and fourth cycles, in spontaneous decomposition of siderite from Fe_3O_4-C-CO_2 system

Cycle	Extra substances added	Siderite yield (%)	CO_2 capture capacity (g CO_2/g sorbent)	$FeCO_3$ weight fraction in decomposed sample (216 h)
2	Water, 3 ml	85.48	0.5237	0.62
3	Water, 3 ml	88.89	0.5446	0.43
4	Water, 3 ml	91.27	0.5591	0.22

Table 3 Pore volume and surface area for initial mixture of magnetite and graphite after 2 h of ball milling and after fourth carbonation-calcination cycle

Fe_3O_4+C	Surface area (m^2/g)	Pore volume (cm^3/g)
Initial mixture	7.001	0.023
2 h milled	14.917	0.046
After four cycles	175.393	0.301

carbonation has high probability of success due to not only the compounds present in the decomposed sample are Fe_2O_3 and Fe_3O_4, but also the absorb properties of the material have improved as can be seen in "Porosity analysis and crystallite size".

$$4\,Fe_3O_4(s) + O_2(g) \rightarrow 6Fe_2O_3(s) \quad (7)$$

Carbonation–decomposition cycles

Recyclability of the products of siderite decomposition at room temperature conditions in subsequent carbonation cycles was also studied. The kinetic limitation in the second carbonation cycle was reduced by adding a considerable amount of water (3.0 ml) per 3.00 g of regenerated iron oxides. Carbonation reaction was studied at 30 bar CO_2 pressure, 400 rpm and for 36 h. Table 2 shows the extra substances added, siderite yield, CO_2 capture capacity of the sorbent and amount of undecomposed siderite after 216 h of exposure to room temperature condition in second, third and fourth cycles.

The results confirm that the regenerated iron oxides can be re-carbonated. Higher capture capacities are achieved with each subsequent carbonation cycle. After 216 h, absence of siderite is evident, which allows to conclude that siderite decomposition kinetic is enhanced by increasing ball milling (Criado et al. 1988). Here, longer ball milling time generates defects, lowers diffusion distance and increases surface area, (Jagtap et al. 1992) (see Table 3) ease capture and release of CO_2, as it was explained in "Siderite decomposition".

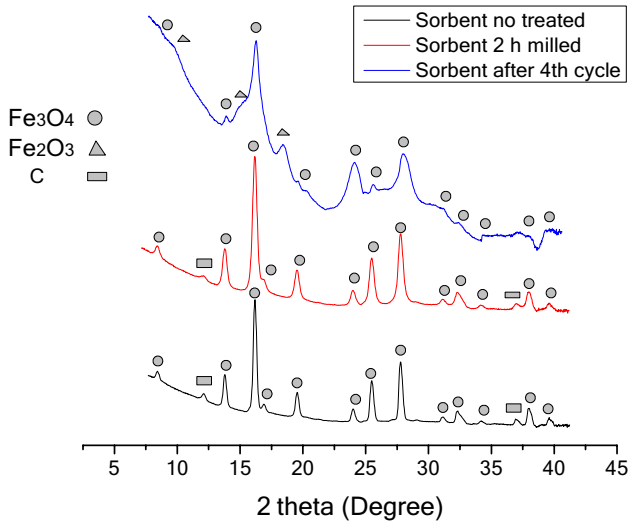

Fig. 7 XRD patterns of initial mixture of initial magnetite and graphite mixture, after 2 h of milling and after of the fourth cycle

Porosity analysis and crystallite size

It has been demonstrated that carbonation of iron oxides is accelerated in the presence of water (Kumar et al. 2015b; Mora et al. 2019b). Furthermore, high efficiency and high capacity of CO_2 capture by iron oxides and iron ore have been accomplished by mechanochemical reactions (Mora et al. 2019a, b). These results have been attributed among others to the surface properties of material. Table 3 presents surface area and pore volume of initial mixture of magnetite and graphite, after 2 h of planetary ball milling and after the fourth cycle of carbonation-decomposition, evidencing that larger surface area and bigger pore volume which are gained by exposing the material to longer milling time allows to improve the sorbent properties.

Additionally, Fig. 7 shows three XRD patterns of initial mixture, after 2 h of milling and after of the fourth cycle. Broadening of diffraction peaks of magnetite during milling indicates about crystallite size reduction. Average crystallite sizes of magnetite in three samples are 112 Å, 78 Å and 45 Å respectively. These sizes are consistent with the reported in other works that synthesized iron carbonate from iron oxides by ball milling process (Mora et al. 2019a).

Kinetic model of siderite decomposition

Kinetics of siderite decomposition at room conditions was studied. Figure 8 plots the siderite conversion fraction as a function of time in first and fourth decarbonation cycles. For the same reaction time, a slightly higher siderite conversion fraction is observed in fourth cycle that can be attributed to a longer total milling time with increasing carbonation/decomposition cycle number. Siderite moves to lower energy expenses by increasing milling time (Kumar 2014).

Obtained kinetic data were fitted to different solid-state reaction mechanism models (Feng et al. 2011; Gotor et al. 2000; Luo et al. 2016; Zakharov and Adonyi 1986). The best fit was obtained for geometrical contraction models, R2 and R3. Results of fitting are illustrated by Fig. 9. Geometrical contraction models assume that nucleation occurs rapidly on the surface of the crystal. The rate of reaction is controlled by the resulting reaction interface progress toward the center of the crystal. Depending on crystal shape, different mathematical models may be derived. In the current study we tested the contracting cylinder (R2) and the contracting sphere/cube (R3) models. As seen in Fig. 9, R2 model provides slightly better fit of experimental kinetic data compared with R3 model. Reaction constants for R2 and R3 models in first and fourth decomposition cycles are provided in the Fig. 9. It is worth noticing small increase of reaction constant in the fourth cycle decomposition reaction compared to the first cycle reaction which can be attributed to particle size reduction and surface area increase.

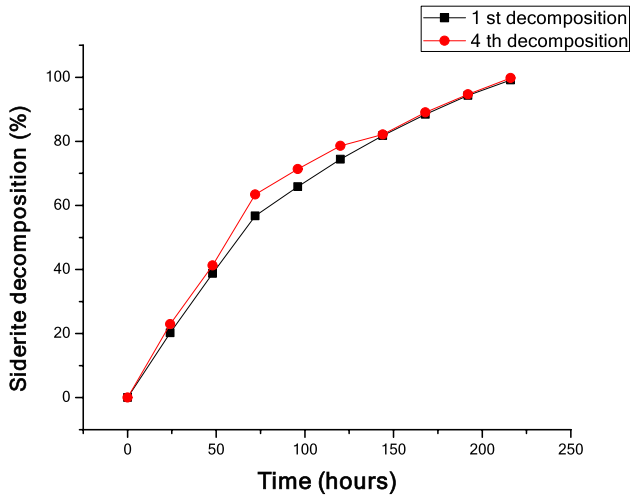

Fig. 8 Siderite conversion factor at room temperature conditions as a function of time in first and fourth carbonation/decomposition cycles

Conclusion

Siderite was synthesized by mechanochemical reactions from magnetite and graphite at 30 bar CO_2 pressure, 400 rpm and 36 h of reaction time in the presence of water. Use of this reaction for carbon dioxide capture is suggested and discussed. Such a sorbent (magnetite and carbon mixture) has CO_2 capture capacity of 0.4829 g CO_2/g sorbent capacity that corresponds to 78.82% of theoretical conversion. It was found that synthesized $FeCO_3$ is unstable at room temperature conditions and ambient atmosphere. Complete decomposition takes around 9 days

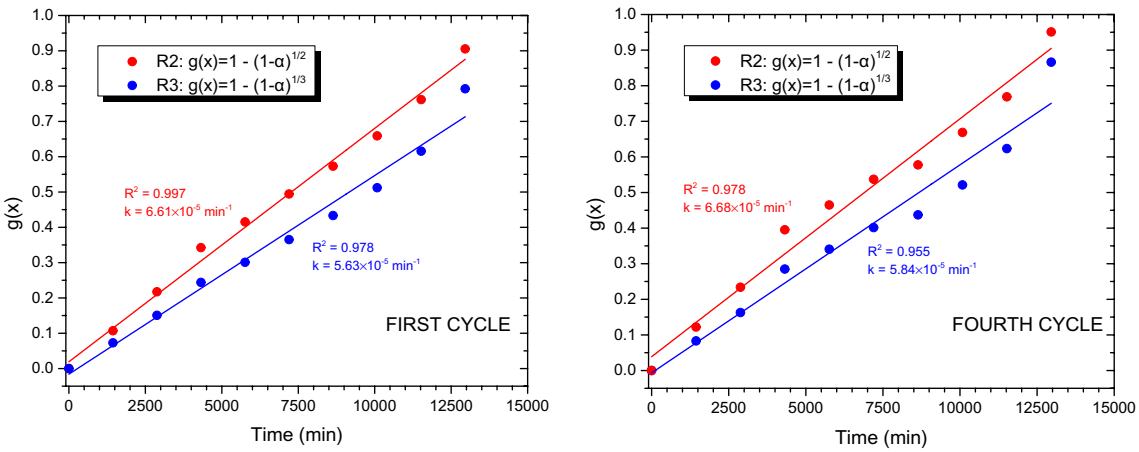

(a) **(b)**

Fig. 9 The integral reaction rate vs. time for siderite decomposition after first (**a**) and fourth (**b**) carbonation cycle. The scattered plots represent the experimental points while the solid lines represent the straight line fit for the contracting cylinder (red) and contracting sphere/cube (blue) solid state reaction mechanism models

yielding magnetite and hematite. The kinetics study shows that the decomposition reaction obeys geometrical contraction model. Cycling stability of the sorbent was tested in four carbonation–decomposition cycles and it was found that the sorbent CO_2 capacity increases with cycle number because of the reduction in the particle size, increase of the surface area and surface activation.

Declarations

Conflict of interest On behalf of all authors, the corresponding author states that there is no conflict of interest.

References

Alkaç V, Atalay Ü (2008) Kinetics of thermal decomposition of Hekimhan-Deveci siderite ore samples. Int J Miner Process 87:120–128

Bale C, Chartrand P, Degterov S, Eriksson G, Hack K, Ben Mahfoud K, Melancon J, Pelton A, Petersen S (2002) Factsage thermochemical software and databases. Calphad 26:189–228

Bello V, Idem R (2005) Comprehensive study of the kinetics of the oxidative degradation of CO_2 loaded and concentrated aqueous monoethanolamine (MEA) with and without sodium metavanadate during CO_2 absorption from flue gases. Ind Eng Chem Res 45:2569–2579

Breckenridge W, Holiday A, Ong J O, Sharp C (2000) Use of SELEXOL process in coke gasification to ammonia project: In Proceedings ofthe Laurance Reid Gas Conditioning Conference. pp397-418

Chai NAL (1994) Enthalpy of formation of siderite and its application in phase equilibrium calculation. Am Mineral 79:921–929

Cheng-Hsiu Y, Huang C-H, Tan C-S (2012) A review of CO_2 capture by absorption and adsorption. Aerosol Air Qual Res 12:745–769

Criado J, Gonzalez M, Macias M (1988) Influence of grinding of both the stability and thermal decomposition mechanism of siderite. Thermochimica 135:219–223

Cullinage T, Rochelle G (2004) Carbon dioxide absorption with aqueous potassium carbonate promoted by piperazine. Chem Eng Sci 59:3619–3630

Das S (2016) Temperature-induced phase and microstructural transformations in a synthesized iron carbonate (siderite) complex. Mater Des 92:189–199

Ding J, Miao W, Pirault E, Street R, Mc Cormick P (1998) Structural evolution of Fe + Fe_2O_3 during mechanical milling. J Magn Magn Mater 177:933–934

Feng Z, Yu Y, Liu G, Chen W (2011) Kinetics of the thermal decomposition of wangjiatan siderite. J Wuhan Univ Technol Matter 1:523–526

Figueroa, Fout T, Plasynski S, Srivastava R (2008) Advances in CO_2 capture technology—the U.S. Department of Energy's Carbon Sequestration Program. Int J Greenhouse Gas Control 2:9–20

Folger P (2013) Carbon capture: a technology assessment, de congressional research service report. University of Nebraska, Lincoln

Fosbøl P, Thomsen K, Stenby H (2010) Review and recommended thermodynamic properties of $FeCO_3$. Corros Eng Sci Technol 45:114–135

Gallagher P, Warne SJ (1981) Thermomagnetometry and thermal decomposition of siderite. Thermochimca 43:253–267

Gheisari K, Javadpour S, Oh J, Ghaffari M (2009) The effect of milling speed on the structural properties of mechanically alloyed Fe–45%Ni powders. J Alloy Compd 472:416–420

Gotor F, Macías M, Ortega A, Criado J (2000) Comparative study of the kinetics of the thermal decomposition of synthetic and natural siderite samples. Phys Chem Minerals 27:495–503

Hammersley AP (1997) FIT2D: an introduction and overview. European Synchrotron Radiation Facility Internal Report ESR-F97HA02T, 68-58.

Han Y, Winston Ho W (2018) Recent advances in polymeric membranes for CO_2 capture. Chin J Chem Eng 26:2238–2254

Han K, Ahn CK, Su Lee M (2014) Performance of an ammonia-based CO_2 capture pilot facility in iron and steel industry. Int J Greenhouse Gas Control 27:239–246

Jagtap S, Pande A, Gokarn A (1992) Kinetics of thermal decomposition of siderite: effect of particle size. Int J Miner Process 36:113–124

Kang S (2020) First-principles evaluation of the potential of using Mg_2SiO_4, Mg_2VO_4, and Mg_2GeO_4 for CO_2 capture. J CO2 Utiliz 42:101293

Kumar S (2014) The effect of elevated pressure, temperature and particles morphology on the carbon dioxide capture using zinc oxide. J CO2 Utiliz 8:60–66

Kumar S, Saxena S (2014) A comparative study of CO_2 sorption properties for different oxides. Mater Renew Sustain Energy 3:1–15

Kumar S, Saxena S, Drozd V, Durygin A (2015a) An experimental investigation of mesoporous MgO as a potential pre-combustion CO_2 sorbent. Mater Renew Sustain Energy 4–8

Kumar S, Drozd V, Durygin A, Saxena S (2015b) Capturing CO_2 Emissions in the Iron Industries using a Magnetite-Iron Mixture. Energ Technol. https://doi.org/10.1002/ente.201500451

Larson A, Von Dreele R (2004) General structure analysis system (GSAS). Los Alamos National Laboratory REport LAUR, pp 87–748

Luo Y, Zhu D, Pan J, Zhou X (2016) Thermal decomposition behaviour and kinetics of Xinjiang siderite ore. Miner Process Extr Metall 125:17–25

Merkel T, Lin H, Wei X, Baker R (2009) Power plant post-combustion carbon dioxide capture: an opportunity for membranes. J Membr Sci 359:126–139

Mora E, Sarmiento A, Vera E, Drozd V, Durygin A, Chen J, Saxena S (2019a) Iron oxides as efficient sorbents for CO_2 capture. J Market Res 8:2944–2956

Mora E, Sarmiento A, Vera E, Drozd V, Durygin A, Chen J, Saxena S (2019b) Siderite formation by mechanochemical and thermo pressure processes for CO_2 capture using iron ore as initial sorbent. Procesess. https://doi.org/10.3390/pr7100735

Pannoccia G, Puccini M, Seggiani M, Vitolo S (2007) Experimental and modeling studies on high-temperature capture of CO_2 using lithium zirconate based sorbents. Ind Eng Chem Res 46:6696–6706

Patterson J (1994) A review of the effects of minerals in processingof Auatralian oil shales. Fuel 73:321–327

Salvador C, Lu D, Anthony D, Abadanes J (2003) Enhancement of CaO for CO_2 capture in an FBC environment. Chem Eng J 96:187–196

Song C, Liu V, Qi Y, Chen G (2019) Absorption-microalgae hybrid CO_2 capture and biotransformation strategy—a review. Int J Greenhouse Gas Control 88:109–117

Stewart C, Hessami MA (2005) Study of methods of carbon dioxide capture and sequestration—the sustainability of a photosynthetic bioreactor approach. Energy Convers Manage 46:403–420

Toby B (2001) EXPGUI, a graphical interface for GSAS. J Appl Cryst 34:210–221

Xie V, Fu Q, Quiao G, Webley P (2019) Recent progress on fabrication methods of polymeric thin film gas separation membranes for CO_2 capture. J Membr Sci 572:38–60

Yan H, Xu Z, Fan M, Bland A, Wright I (2008) Progress in carbon dioxide separation and capture: a review. J Environ Sci 20:14–27

Yang Y, Xu X, Guo Y, Wood C (2020) Enhancing the CO_2 capture efficiency of amines by microgel particles. Int J Greenhouse Gas Control 103:103172

Zakharov V, Adonyi Z (1986) Thermal decomposition kinetics of siderite. Thermochim Acta 102:101–107

Zaman M, Lee JH (2013) Carbon capture from stationary power generation sources: a review of the current status of the technologies. Korean J Chem 30:1497–1526

Zhang J, Webley P (2008) Cycle development and design for CO_2 capture from flue gas by vacuum swing adsorption. Environ Sci Technol 42:563–569

Zhang N, Pan Z, Zhang Z, Zhang W, Zhang L, Baena-Moreno F, Lichtfouse E (2010) CO_2 capture from coalbed methane using membranes: a review. Environ Chem Lett 18:79–96

Zhou GT (2011) Synthesis of siderite microspheres and their transformation to magnetite microspheres. Eur J Mineral. https://doi.org/10.1127/0935-1221/2011/0023-2134